Research Article | Vol. 12, No. 11 / 1 Nov 2021 / Biomedical Optics Express 6831
Biomedical Optics EXPRESS

Discriminating turbid media by scatterer size and scattering coefficient using backscattered linearly and circularly polarized light

MICHAEL D. SINGH[1] AND I. ALEX VITKIN[1,2,3,*]

[1]Department of Medical Biophysics, University of Toronto, Toronto, ON, Canada
[2]Department of Radiation Oncology, University of Toronto, Toronto, ON, Canada
[3]Division of Biophysics and Bioimaging, Princess Margaret Cancer Centre, Toronto, ON, Canada
[*]Alex.Vitkin@rmp.uhn.ca

Abstract: The effects of scatterer size and scattering coefficient on backscattered linearly and circularly polarized light are investigated through Stokes polarimetry. High-SNR polarization modulation/synchronous detection measurements are corroborated by polarization-sensitive Monte Carlo simulations. Circular degree of polarization (DOP) is found to be sensitive to scatterer size, but is equivocal at times due to helicity flipping effects; linear DOP appears to be mostly dependent on the medium scattering coefficient. We exploit these trends to generate a DOP_C - DOP_L response surface which clusters turbid samples based on these medium properties. This work may prove useful in biomedicine, for example in noninvasive assessment of epithelial precancer progression.

1. Introduction

Turbid media scatter light in interesting and characteristic ways that can convey information about its properties. When polarized light encounters a heterogeneous medium, the primary modulation mechanism is polarization decoherence (commonly referred to as depolarization) whereby the collectively shared phases and amplitudes of the incident photons' electric field components are decorrelated and randomized during scattering [1]. Additionally, when polarized light is backscattered from a medium, another modulation mechanism becomes prominent, that of orthogonal flipping of the incident polarization orientation (e.g., right-circular polarization converts to left-circular polarization). Measuring backscattered light is integral for polarized light assessment of tissue *in vivo* [2] due mainly to the significantly limited polarimetric sampling depth (a few millimeters at most [3]) which is not conducive for transmission through bulk tissue. The mechanisms of polarization decoherence and orientational flipping can be indicative of a medium's scattering coefficient (essentially its turbidity) and scatterer size distribution, thus enabling backscattered polarized light to probe these two biophysically important sample properties. For example, during epithelial precancer-to-cancer progression, changes occur to both tissue turbidity and average scatterer size as cells undergo morphological changes to their nuclear size (pleomorphism) and concentration (cellular proliferation) [4–7]. Thus, backscattered polarized light may be used to noninvasively detect epithelial precancers *in vivo*, an improvement to the current invasive and subjective *ex-vivo* assessment by tissue biopsy [8,9]. Furthermore, polarimetric optical diagnostics of scatterer properties may also benefit photodynamic therapy, a variant of which employs photosensitive nanoparticles to treat cancers [10], where there is a need for assessing photosensitizer concentration and aggregation [11]. Therefore, a noninvasive *in-vivo* ability to assess scatterer size distributions and scattering coefficient may prove important in biomedicine, and polarized light is promising for this task through its characteristic polarization responses, particularly in the biomedically important backscattering detection geometry.

#438631 https://doi.org/10.1364/BOE.438631
Journal © 2021 Received 23 Jul 2021; revised 22 Sep 2021; accepted 3 Oct 2021; published 11 Oct 2021

Biomedical Optics EXPRESS

Prior to *in-vivo* biomedicine however, many fundamental and practical aspects of the enabling polarimetric methodology must be assessed and optimized. In this study, we thus rigorously examine the polarization responses of backscattered linearly and circularly polarized light in a model system composed of uniform-sized spherical microparticles suspended in a liquid, simulating cell nuclei in tissue and simplifying the light interaction dynamics. Broadly speaking, back-scattered light from such a suspension of particles consists of two subpopulations of photons: type-1 – those that have undergone a reflection-like backscattering event by a single scatterer (large scattering angle, possibly approaching 180°) at some depth in the medium, and type-2 – those that have been forward-scattered at small scattering angles multiple times and eventually redirected into the backwards hemisphere direction (i.e., no single reflection-like scattering event) [12–16]. Importantly, polarized light encodes information about both of these backscattering routes through polarization decoherence and orientational flipping mechanisms. Specifically, circularly polarized light undergoes a helicity flip after a reflection-like event (type-1) whereby its initial and scattered polarization states are related by mirror symmetry (e.g., incident right circularly polarized light emerges as left circularly polarized light). In contrast, circular polarization helicity is preserved after forward scattering (type-2 subpopulation) and possibly measurable due to the resultant modest circular depolarization effects [12,17]. Linear states, however, effectively depolarize with the randomization of their photon's directions [18]; hence, the multiply scattered redirected backscattering (type-2) sub-population will be greatly depolarized compared to the minimally scattered type-1 photons. In addition to geometric (randomization) processes, so-called "dynamical" depolarization effects have been explored in detail; the reader may refer to [19–21] for largely analytical treatment of these problems. In general, these considerations suggest that one can gain insight into the complexities of the light-medium interactions and by analyzing the behaviour of backscattered linearly and circularly polarized light.

Relating these interactions to medium properties, we note that both scatterer size and scattering coefficient will influence the relative contributions of type-1 and type-2 backscattered photon interactions. Particles large compared to the interrogating light's wavelength (Mie regime) scatter predominantly in the forward direction, thus increasing the relative contribution of type-2 backscattered photons; this may lead to preferential retention of helicity-maintaining circularly polarized light fraction. Conversely, smaller sized scatterers (Rayleigh regime), with their more symmetric backward-forward scattering patterns, increase the relative probability of directly reflected type-1 photons; this may favour linear polarization preservation over the helicity-flipped circular subpopulation. The influence of scattering coefficient is somewhat less clear, other than the general expectation that degree of polarization (DOP) should overall decrease with increasing turbidity [22]. For example, it has been suggested that low turbidity (such as that of eye) backscatters mainly type-1 photons and high turbidity (such as that of tissue epithelia) backscatters mainly type-2 photons [13]; however, these effects should be further explored. Overall then, a careful rigorous study of backscattered polarization effects in media with well-defined scatterer sizes and scattering coefficients will provide insight into the polarimetric probing capabilities for assessing these two biophysically important parameters.

The detailed polarization responses from turbid media were first observed in a seminal 1989 study by MacKintosh *et al.* [12] who investigated the effects of scatterer size on linearly and circularly polarized light and found a stronger circular "polarization memory" for Mie (larger) scatterers and stronger linear polarization memory for Rayleigh (smaller) scatterers. This study sparked a strong research interest in linearly and circularly polarized light and their interactions with simple scattering media (particle suspensions) [14–19,23–28], including on the question of which polarization state is better preserved under various experimental conditions (such as medium properties and measurement geometry). These have largely supported the initial observations of linear and circular polarization retention with respect to scatterer size from the

Biomedical Optics EXPRESS

MacKintosh study. However, there have also been contrary observations in backscattered light from more complex media such as tissue phantoms with roughened surfaces, polydispersed suspensions of aspherical particles, and actual biological tissues [29–37]; here the optical properties are less understood which make it difficult to determine the underlying reason(s) for these contradictory results. Effects of speckle, absorption, polydispersity [38], or preferential interactions with smaller scatterers have been invoked; however, as noted recently [33], this issue deserves further investigation. There is thus a strong need to better understand backscattered polarized light to gain clarity on the question of linear versus circular polarization preservation in media of different scatterer size distributions and turbidity, particularly to facilitate the development of polarimetric techniques that aim to utilize these polarization states on bulk tissue such as cancer detection and assessment [33,34,39] and optical sampling depth sensitivity [40–42].

Here we attempt to gain insight on these issues by studying backscattered polarized light within the context of the type-1 and type-2 interaction media. This model enables us to better understand the light-medium interactions based on the characteristic polarization modulations discussed above, namely, the helicity response of circularly polarized light (flipped for type-1 and preserved for type-2) and linear DOP (non-zero for type-1 and effectively zero for type-2). Furthermore, since backscattering experiments typically measure differences between polarization intensities of orthogonal states, an ambiguity arises when the resultant circular DOP is low. Is it because the light field is 'truly' random and depolarized, or is significant polarization coherence present but masked by the presence of roughly similar amounts of orthogonal states (helicity-preserved and helicity-flipped)? Resolving this interesting ambiguity is also worthy of further investigation and may help provide insight on the much-discussed question of linear versus circular polarization preservation.

In this study, we thus investigate the responses of backscattered linearly and circularly polarized light in controlled turbid media of varying scatterer sizes and scattering coefficients to better understand their relationships with these medium properties, while also providing insight on the issue of ambiguous circular polarization Stokes measurements. The findings enable a novel polarimetric methodology to discriminate turbid media simultaneously by scatterer size and scattering coefficient. To perform the measurements, we employ a practical high-SNR experimental system with dynamic polarization modulation and phase-sensitive synchronous detection, which requires only a single input polarization configuration to measure both linear and circular responses. We also present simulation results from a polarization-sensitive Monte Carlo model to validate the experimental measurements, help resolve the low DOP_C ambiguity, and provide additional insights (e.g., scattering interaction numbers within the scattering volume).

2. Methods

2.1. Turbid media samples

The turbid samples were aqueous suspensions of monodispersed polystyrene microspheres (Bangs Laboratories, Inc) of different sizes and scattering coefficients. Three sphere diameters were used – 0.21 μm, 0.42 μm, and 0.96 μm – which at $\lambda = 635$ nm yield scattering efficiencies Q and scattering anisotropy factors g as (0.08, 0.35), (0.52, 0.74) and (2.45, 0.92), respectively, as calculated by Mie theory [43]. The spheres had a refractive index of $n = 1.59$. Concentrations were varied to yield scattering coefficients ranging from $\mu_s = 5\ \text{cm}^{-1}$ to $\mu_s = 200\ \text{cm}^{-1}$. Aqueous suspensions were placed into a plastic cuvette with a 1×1 cm silica optical window.

2.2. Experimental system and signal analysis

Figure 1 shows the schematic for the experimental system. The light source was a continuous-wave diode laser operating at $\lambda = 635$ nm. The light was modulated sequentially by a mechanical

Biomedical Optics EXPRESS

chopper at 207 Hz, linear polarizer (P1), and photoelastic modulator (PEM) before impinging on the sample. We can describe the polarization states of light in the form of Stokes vectors [44],

$$S = \begin{bmatrix} \mathrm{I} \\ \mathrm{Q} \\ \mathrm{U} \\ \mathrm{V} \end{bmatrix} = \begin{bmatrix} \mathrm{I_H} + \mathrm{I_V} \\ \mathrm{I_H} - \mathrm{I_V} \\ \mathrm{I_{+45}} - \mathrm{I_{-45}} \\ \mathrm{I_R} - \mathrm{I_L} \end{bmatrix}. \tag{1}$$

where $\mathrm{I_H}$, $\mathrm{I_V}$, $\mathrm{I_{+45}}$, $\mathrm{I_{-45}}$, $\mathrm{I_R}$, and $\mathrm{I_L}$ are the light intensities measured by a horizontal linear analyzer, a vertical linear analyzer, a linear analyzer oriented at +45°, and linear analyzer oriented at −45°, a right circular analyzer, and a left circular analyzer before reaching the detector, respectively.

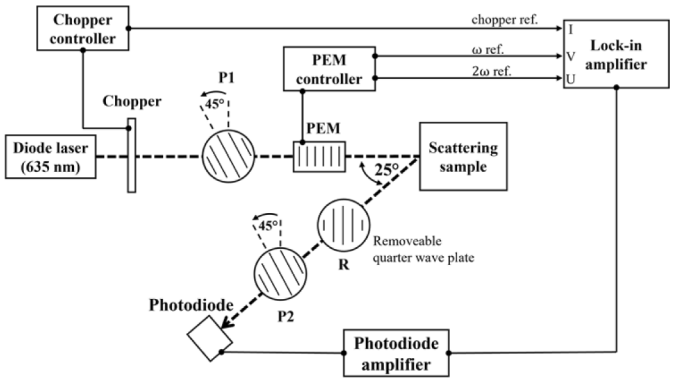

Fig. 1. Schematic of the experimental system used to measure the Stokes parameters I, U, and V from scattering samples. P1 is a linear polarizer with its optical axis oriented at 45° counterclockwise from the vertical when viewing from the incident side, the birefringent axis of the PEM is oriented vertically, R is a quarter wave retarder with its fast axis oriented vertically and P2 is a linear polarizer with its optical axis oriented 45° clockwise from the vertical. R was placed in the beam path to form a circular analyzer and removed to expose the linear analyzer. To measure the incident light properties, the sample was removed and the detection axis was swivelled parallel to the beam line.

The state of light after transmitting through P1 is represented as

$$S_1 = I_{in} \begin{bmatrix} 1 \\ 0 \\ 1 \\ 0 \end{bmatrix}, \tag{2}$$

here I_{in} is the initial intensity of the light (reduced by half by the mechanical chopper). The PEM (Hinds PEM-90) consisted of a slab of quartz with an oscillatory strained birefringence. The Stokes vector of the light after transmitting through the PEM is found by taking the product of

Biomedical Optics EXPRESS

the PEM's Mueller matrix and $\boldsymbol{S}_1$,

$$\boldsymbol{S}_2 = \begin{bmatrix} 1 & 0 & 0 & 0 \\ 0 & 0 & 0 & 0 \\ 0 & 0 & \cos\delta & \sin\delta \\ 0 & 0 & -\sin\delta & \cos\delta \end{bmatrix} \boldsymbol{S}_1 = I_{in} \begin{bmatrix} 1 \\ 0 \\ \cos\delta \\ -\sin\delta \end{bmatrix}. \tag{3}$$

The retardation of the PEM, δ, varies sinusoidally with time at frequency $f = \omega/2\pi$,

$$\delta = \delta_o \cos(\omega t), \tag{4}$$

where δ_o is the user-selected peak retardance. The cos δ and sin δ terms can then be expanded in terms of Bessel functions,

$$\cos\delta = \cos(\,\delta_o \cos(\omega t)\,) = J_0(\delta_o) - 2J_2(\,\delta_o)\cos(2\omega t) + \ldots, \tag{5}$$

$$-\sin\delta = -\sin(\,\delta_o \cos(\omega t)\,) = -2J_1(\delta_o)\cos(\omega t)\,) + 2J_3(\delta_o)\cos(3\omega t)\,) + \ldots. \tag{6}$$

To simplify analysis, we set the peak PEM retardance δ_o to 2.405 rad where $J_0(\delta_o) = 0$ (see Eqn. (5)). With this simplification, the PEM-transmitted light oscillated between right- and left-circularly polarized light at the fundamental frequency ω (with amplitude $2J_1$) and between +45° and −45° linearly polarized light at the harmonic frequency 2ω (with amplitude $2J_2$).

The light is then scattered in the turbid sample, represented by the product of the Mueller matrix of a depolarizer and $\boldsymbol{S}_2$:

$$\boldsymbol{S}_3 \propto \begin{bmatrix} 1 & 0 & 0 & 0 \\ 0 & \mathrm{DOP_L} & 0 & 0 \\ 0 & 0 & \mathrm{DOP_L} & 0 \\ 0 & 0 & 0 & \mathrm{DOP_C} \end{bmatrix} S_2 = \begin{bmatrix} 1 \\ 0 \\ \mathrm{DOP_L}\cos\delta \\ -\mathrm{DOP_C}\sin\delta \end{bmatrix} = \begin{bmatrix} 1 \\ 0 \\ 2J_2\mathrm{DOP_L}\cos(2\omega t) \\ -2J_1\mathrm{DOP_C}\cos(\omega t) \end{bmatrix} \tag{7}$$

where $\mathrm{DOP_L}$ is the linear DOP, and $\mathrm{DOP_C}$ is the circular DOP.

The light was measured before scattering and after scattering by swiveling the detection axis parallel to the beam line in the former case and to 25° with respect to the incident beam in the latter case (25° was the closest-to-180° angle permitted by the optics). An off-axis backscatter detection geometry was chosen as an alternative to exact backscattering to avoid the use of a beam splitter which both complicates the Mueller matrix mathematics and reduces the measurable intensity [22]. The details of Stokes measurements using photoelastic modulation and synchronous detection are available in previous rigorous publications [45–49]. Briefly, the Stokes parameters I, U, and V are measured using a lock-in amplifier [50] by detecting the photodiode signal synchronously with the chopper reference signal (DC intensity, or I), the fundamental (ω) PEM reference signal, and the harmonic (2ω) PEM reference signal, respectively. The fractional linear polarization, U/I, and fractional circular polarization, V/I, of the scattered light are normalized by that of the incident light to obtain $\mathrm{DOP_L}$ and $\mathrm{DOP_C}$,

$$\frac{\mathrm{U}_{out}/\mathrm{I}_{out}}{\mathrm{U}_{in}/\mathrm{I}_{in}} = \mathrm{DOP_L}, \tag{8}$$

$$\frac{\mathrm{V}_{out}/\mathrm{I}_{out}}{\mathrm{V}_{in}/\mathrm{I}_{in}} = \mathrm{DOP_C}, \tag{9}$$

where the "*out*" subscript denotes the scattered components and the "*in*" subscript denotes the incident components. Both $\mathrm{DOP_L}$ and $\mathrm{DOP_C}$ can range from −1 to +1 where negative values

Biomedical Optics EXPRESS

indicate a flip of the incident orientation to its orthogonal state and positive values indicate preservation of the incident orientation.

Notably, the above-described method whereby the scattered polarization fractions are normalized by the incident polarization fractions, enabled the measurement of both linear and circular DOPs using a fixed PEM-enabled incidence. This simplified the measurement process and reduced the chance of experimental error. In this direct experimental approach, the diffusive component of the backscattered light is gated out, leading to high-SNR detection of primarily ballistic (type-1) and snake (type-2) photons which are important in retaining physical information from interrogated media. As shown in several previous studies [14,51,52], such continuous-wave phase modulation polarization gating rather than temporal polarization gating obviates the need for complex and expensive ultrashort-pulsed lasers and rapid-response detectors such as streak cameras [53–55]. To make the measurement system even faster and more robust, the quarter wave retarder on the detection side can be replaced by another PEM to enable fully no-moving-parts measurement of U and V [49]. Such a robust and rapid two-PEM based experimental system without mechanically moving parts would be well suited for the challenges of reflection-mode bulk tissue *in-vivo* polarimetry, furnishing excellent phase-sensitive detection sensitivity [56] to address severe tissue depolarization and enables rapid signal acquisition times to minimize motion artifacts [3].

2.3. Monte Carlo model

We employed our previously developed, validated and publicly available Monte Carlo model [57] to simulate polarized light propagation in multiply scattering media. The model corroborated the experimental DOP measurements and tracked the average number of scattering events per detected photon (including both polarization-retaining and depolarized populations), thus offering insights into the backscattering mechanisms and facilitating data interpretations.

The relevant aspects of the polarization-sensitive Monte Carlo model are briefly summarized here, with detailed description, validation and usage previously published [58]. The model tracks the position, direction, and polarization via Stokes vectors of photons as they propagate through a scattering medium and sums the photon histories to determine the macroscopic polarization properties of the scattered light. Each photon takes on a new propagation direction after a scattering event by determining the scattering angle through statistical sampling. The Stokes vector of each photon is transformed via the Mueller matrix of each scattering event as calculated by Mie theory. Upon encountering a sample boundary, reflection or transmission probabilities are calculated from the polarization-dependent Fresnel coefficients; reflected photons continue their propagation in the medium with their properties transformed accordingly. A fraction of scattered photons escapes the medium and impinges on a detector element at a specific measurement angle (25° off the retroreflection direction in our study) and surface area (5 cm^2 in our study), yielding a summation of the detected photon statistics.

Each simulation was initialized with parameters matching the experimental setup which describe the detection geometry, the medium properties (scatterer size and refractive index, host medium refractive index, scattering coefficient, and medium dimensions), and incident light properties (polarization, number of photons ($\sim 10^8$), and wavelength). The incident state of light was initialized with the same Stokes parameters as the experimentally measured excitation light onto the sample. A typical simulation took ~20 minutes on a laptop PC with an Intel Core i5-7200U 2.71 GHz processor. Stokes DOP_L and DOP_C fractions were calculated same as in the experimental methodology, by normalizing the linear and circular polarization fractions of the scattered light by that of the incident light.

Biomedical Optics EXPRESS

3. Results and discussion

We first investigate the effects of scatterer size on DOP_L and DOP_C. Plotted along the left vertical axis in Fig. 2 are the simulated and experimental DOP_L and DOP_C values for monodispersed suspensions with sphere diameters ranging from 0.21 μm to 0.96 μm, all with the scattering coefficient kept constant at μ_s = 100 cm^{-1} (mean free path (MFP) = $1/\mu_s$ = 0.01 cm). The scattering anisotropy of each mean sphere diameter is plotted along the top horizontal axis. Experimental measurements were performed for suspensions of 0.21 μm, 0.42 μm, and 0.96 μm diameter spheres; d = 0.6 and 0.8 μm were added in the simulations. The experimentally measured DOP curves are corroborated by the Monte Carlo simulation results, showing strong agreement and lending credence to the observed trends. The red curve on the right vertical axis of Fig. 2 displays the corresponding Monte Carlo calculated average number of scattering events detected in the backscattering direction for the different sphere sizes at μ_s = 100 cm^{-1}. As seen, the average number of scattering events increases with sphere diameter, which can be attributed to the stronger forward scattering of larger spheres, leading to higher relative contributions of the multiply scattered type-2 photons. As such, DOP_C also increases with sphere diameter since type-2 photons are helicity-preserved and modestly circularly depolarized with increasing scatterer size [12]. Conversely, the type-2 photons are highly linearly depolarized [18] and thus an overall low and slightly decreasing response is observed for DOP_L with particle size, and with far less dynamic range than DOP_C. As expected, the DOP_L signal is maximum for smallest examined microspheres (d = 0.21 μm), which is likely due to the higher preponderance of minimally scattered type-1 photons (g = 0.35) [12]. Interestingly, DOP_L remains non-zero at this high turbidity level for all scatterer sizes; this phenomenon likely arises due to ever-present minimally scattered type-1 photons from shallow layers of the sample [22,59]. Overall we note that DOP_C shows greater sensitivity to medium scatterer size compared to DOP_L, due to its greater dynamic range and more pronounced variation.

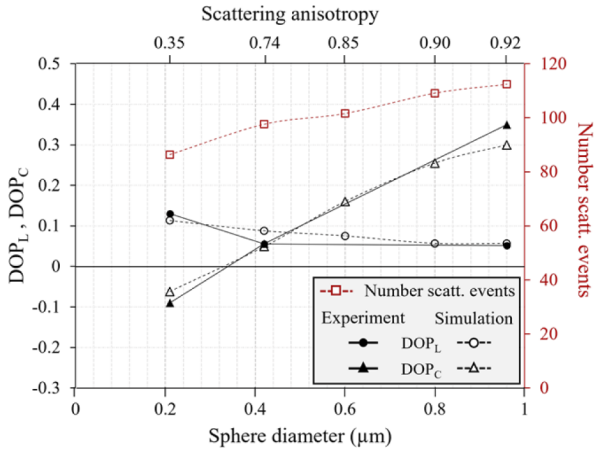

Fig. 2. Simulated and experimentally measured linear DOP_L and circular DOP_C fractions in monodispersed polystyrene suspensions with microsphere diameters ranging from 0.21 μm to 0.96 μm. Each suspension had a scattering coefficient μ_s = 100 cm^{-1} (MFP = $1/\mu_s$ = 0.01 cm). The corresponding scattering anisotropy for each microsphere diameter is plotted along the top horizontal axis (not to scale). Experimental results are presented for suspensions of 0.21 μm, 0.42 μm, and 0.96 μm diameter spheres; Monte Carlo simulations also show d = 0.6 μm and 0.8 μm results. The red symbols and the right vertical axis show the average number of scattering events per detected photon for each simulation run. Solid symbols = experimental results; hollow symbols = Monte Carlo simulation results; lines = guide for the eye.

Biomedical Optics EXPRESS

However, we also note that the trendline of DOP_C intersects zero at approximately d = 0.3 μm (g = 0.65), which can be interpreted as either (a) circular decoherence or (b) a condition where the helicity-preserved intensity roughly equals the helicity-flipped intensity whereby the corresponding $V = I_R - I_L$ measurement yields ~ zero. We posit that the latter is the true mechanism, based on (a) the overall continuity of the DOP_C curve, (b) the non-zero value of DOP_L for sphere diameter of 0.3 μm which indicates that the minimally scattered and polarization preserving type-1 photons are present, and (c) some degree of backscattered polarization will theoretically always remain due to the aforementioned shallow-layer backscattering [60]; thus, total decoherence of circular polarization is unlikely despite $DOP_C \sim 0$. Furthermore, this ambiguity was directly observed, although not pointed out, by MacKintosh *et al.* [12] who measured separate signals for left- and right-circular polarization intensities of backscattered light from monodispersed polystyrene microsphere suspensions and showed that the two signals take on ~equal non-zero magnitudes at a certain microsphere concentration and average diameter, which would make the Stokes V value = 0 even though considerable circular polarization coherence remained. This ambiguity must be kept in mind when designing / interpreting polarization studies in turbid media, in that circular DOP may appear to be ~ 0 for certain medium properties (specifically scatterer size), despite there being significant underlying circular polarization preservation via two separate but opposite-helicity subpopulations. One useful means to combat this ambiguity would be to quantify and retain the orthogonal polarization intensities, instead of automatically subtracting them, thus preserving rather than degrading the circular polarization information. We note that some previous studies may have missed this mathematical caveat with circular depolarization. For example, Louie *et al.* [33] have recently reported stronger depolarization of circularly than linearly polarized light in tissue phantoms and skin lesions in backscattered Stokes DOP measurements. In fact, these observations may or may not be due to strong circular polarization decoherence, but could also stem from there being closely valued helicity-preserved and helicity-flipped intensities (for example, the tissue phantoms used in their study had scattering anisotropies ranging from g = 0.69 to g = 0.82, close to g = 0.65 where $DOP_C \sim 0$ under our experimental conditions). Similar considerations may need to be invoked in the complex and often conflicting debates of whether linear or circular polarization states are better preserved in particulate phantom media and in tissues.

The increase in the average number of scattering events N with microsphere diameter implies the corresponding increase in the total penetration depth D of the light, estimated here as $D \sim N * MFP * g / 2$ for retroreflection geometry. This however represents the average sampling depth of the entire detected light field, and not specifically the polarization-maintaining fraction, as the relatively large values of N reported here include all detected photons; the average sampling depths of the polarization-preserving fractions are likely somewhat lower [61]. It has also been shown that linearly and circularly polarized light fractions exhibit different depth sensitivities, thus suggesting polarization *ellipticity* as a tuning mechanism for depth selectivity [40–42]. The results in Fig. 2 show that such an approach must consider the scattering anisotropy of the interrogated medium to first determine the difference in polarization retention rates between both polarization states which would in turn affect the depth sensitivities. In fact, there may be no difference at all in some media: for example in Fig. 2 there is an intersection point between DOP_L and DOP_C at sphere diameter of ~0.4 μm, which would preclude the use of an ellipticity tuning mechanism for differential depth discrimination. Here is thus another example of the intricacies surrounding the question of linear versus circular polarization retentions, the insights afforded by careful measurements/analysis and associated modeling, and resultant consequences for potential applications.

We next study the effects of scattering coefficient on DOP_L and DOP_C for suspensions with three different microsphere sizes. Figures 3(a), 3(b), 3(c) show the simulated and experimentally measured DOP_L and DOP_C values (left vertical axes) and simulation-obtained average number of

Biomedical Optics EXPRESS

scattering events per detected photon (right vertical axes) plotted against scattering coefficient for suspensions containing spheres with diameters of 0.21 μm, 0.42 μm, and 0.96 μm, respectively. Strong agreement is observed between the experimental and Monte Carlo simulated DOP curves, again firming up the observed trends. That said, slight discrepancies are evident at lower scattering coefficients (more pronounced for larger spheres and circular polarization; see Fig. 3(c), triangular symbols). The cause of this discrepancy for the more transparent media (μ_s<50 cm^{-1}) is currently being investigated; but since we are primarily interested in higher scattering media of tissue-like levels of turbidity [62], this lower-scattering discrepancy is not consequential for the current discussion.

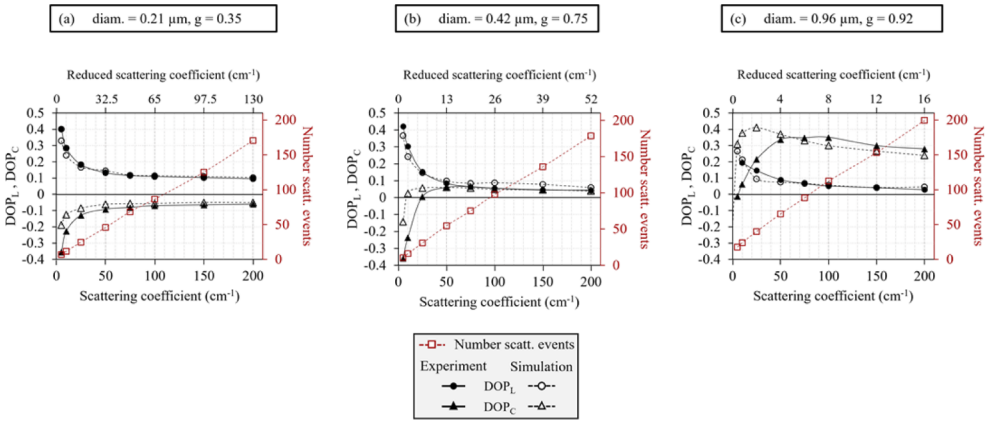

Fig. 3. Simulated and experimentally measured DOP_L and DOP_C signals for monodispersed suspensions with scattering coefficients ranging from 5 cm^{-1} to 200 cm^{-1} and spheres of diameter (a) 0.21 μm, (b) 0.42 μm, (c) 0.96 μm. The red symbols and the right vertical axis show the average number of scattering events per detected photon for each simulation run. Solid symbols = experimental results; hollow symbols = Monte Carlo simulation results; lines = guide for the eye.

The number of scattering events increases with scattering coefficient in each plot in Fig. 3. First focusing on the DOP_C curves for the two larger sphere sizes (Fig. 3(b) and Fig. 3(c)), we note that the increase in the number of scattering events must arise primarily from increased photon redirection (type-2 backscattering) since the DOP_C values increase from negative helicity-flipped signals to positive helicity-preserved signals. In this case, the relative contribution of type-2 light increases with scattering coefficient, whereby correspondingly lower MFPs enhance the mediums' ability to redirect photons back towards the detector. Eventually, the number of scattering events become sufficiently high such that the depolarization effects begin to dominate, manifesting as slight decreases in DOP_C for scattering coefficients > ~60 cm^{-1} and ~100 cm^{-1} (Fig. 3(b) and Fig. 3(c), respectively). Again, we attribute the $DOP_C \sim 0$ level to the difference in orthogonal circular polarization intensities being nullified, and not to the true polarization loss due to decoherence. The small anisotropy factor of the smallest sphere size likely does not strongly support the multiple-forward-scattered photon redirection mechanism [15] regardless of scattering coefficient, thus DOP_C remains helicity-flipped (negative) in Fig. 3(a). In this case, the backscattered intensity primarily consists of type-1 light, and thus we observe an expected simple exponential decay (in magnitude) with the increasing number of scattering events as indicative of polarization decoherence [1] (i.e., not an interplay of helicity-flipped and helicity-preserved intensities as observed in Fig. 3(b) and Fig. 3(c)). Further, since linearly polarized backscattered intensity essentially comprises only type-1 photons, DOP_L curves also exhibit exponentially decaying profiles for all three plots in Fig. 3 (with highest values for the

Biomedical Optics EXPRESS

lowest diameter (lowest g-value) medium of Fig. 3(a)). We thus note that DOP_L is a better predictor of scattering coefficient due to its consistent and simple decaying dependence on it, as opposed to the rise-and-fall behaviour of DOP_C in suspensions of larger scatterers. Again we note that both DOP_L and DOP_C both exhibit non-zero asymptotes with increasing scattering coefficient, thus some polarization information is always preserved in backscattering; this arises from the presence of minimally scattered shallow-layer type-1 photons regardless of increasing medium turbidity.

Since DOP_L and DOP_C were found to exhibit predictive features of scatterer size and scattering coefficient, we generate a parametric plot where experimentally measured pairs (DOP_L, DOP_C) are plotted as shown in Fig. 4. The DOP_L and DOP_C data points are a subset from the results presented in Fig. 2 and Fig. 3, concentrating on the three sphere diameters which have been measured in the lab and on the tissue-relevant range of scattering coefficients, $50\,cm^{-1}$ to $200\,cm^{-1}$. On the resultant response surface, there are visible three distinct clusters which correspond to the three different sphere diameters. We again note that DOP_C exhibits a far wider dynamic range than DOP_L due to its stronger variance with sphere size (see Fig. 2), and thus the size clusters vary mainly along the DOP_C axis. The points in each cluster are differentiated by scattering coefficient along both DOP_L and DOP_C axes, though not as visible on the latter due to its larger scale. However, DOP_L is a better predictor of scattering coefficient based on its simple decaying relationship with scattering coefficient, as opposed to the more complex rise-and-fall behaviour of DOP_C for the two larger sphere suspensions.

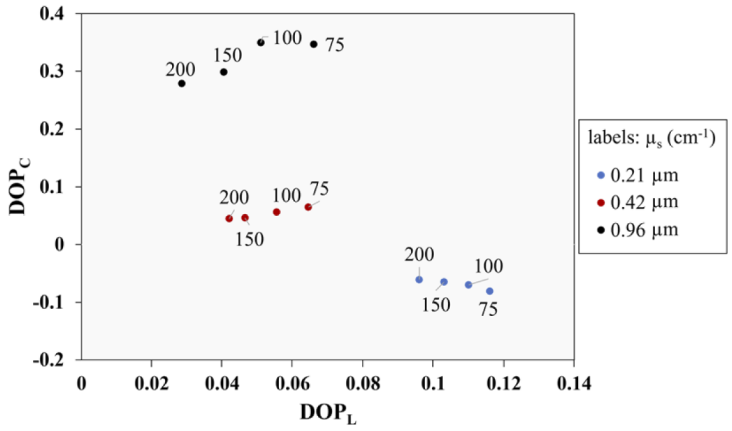

Fig. 4. A $DOP_{L/C}$ response surface for monodispersed microsphere suspensions with a given scattering coefficient (ranging from $50\,cm^{-1}$ to $200\,cm^{-1}$) and mean sphere diameter (0.21 μm, 0.42 μm, and 0.96 μm). Clustering according to particle size (distinct along the DOP_C axis) and scattering coefficient (somewhat along the DOP_L axis) is evident; for details, see text.

It is thus evident that the Stokes measurements of DOP_L and DOP_C are capable of discriminating turbid samples simultaneously by scatterer size and scattering coefficient. The generalizability of these results to a broader parameter space, and their direct applicability to tissue polarimetry, is not yet certain; thus, further investigations are needed in random media with more tissue-like fluctuations in the refractive index and non-uniformly sized/shaped scatterers. Nonetheless, these encouraging early results suggest that once we measure DOP_L and DOP_C of an unknown sample and plot the resultant pair (DOP_L, DOP_C) on a response surface similar to Fig. 4, we will learn something about its dominant scatterer size and the magnitude of its scattering coefficient. Such biophysical insights can indeed prove useful in biological tissue characterization applications, for example in the case of epithelial precancer-to-cancer progression that can exhibit simultaneous

Biomedical Optics EXPRESS

changes to scatterer size distribution (via pleomorphism) and turbidity (via cell proliferation). Plotting measured DOP_L and DOP_C values from these tissues on the response surface such as in Fig. 4 may thus prove helpful in detecting and staging cancers based on the average nuclear size and cellular concentration [5–7]. Additionally, a similar response surface approach may furnish useful assessment information on particulate photosensitizer properties (e.g., aggregation) during photodynamic therapy to improve its efficacy [11].

4. Conclusion

Herein, we investigate the linear and circular polarization responses in media with different scatterer sizes and scattering coefficients by performing Stokes measurements to obtain their degrees of polarization. Circular DOP is found to be sensitive to both sub-populations of backscattered photons – directly reflected and forward-scattered-redirected type – whereas linear DOP shows sensitivity primarily to the former type (due to its depolarization for the latter type interactions). Thus, DOP_C varies (1) significantly with the scatterer size, and (2) complexly with the scattering coefficient, based on the interplay of both types of photons as well as overall depolarization. DOP_C is thus a good marker for scatterer size, but its Stokes backscattering measurements can be ambiguous, arising from either true polarization decoherence or from closely valued orthogonal polarization intensities, or a combination of the two. Linear DOP exhibits a weak dependence on scatterer size in the Mie (larger-scatterers) regime, and a decrease with the scattering coefficient for all scattering diameters. A simple strategy to use linear and circular polarimetry to assess dominant scatterer size and magnitude of the scattering coefficient of an unknown sample is thus presented.

Notably, the backscattered linearly and circularly polarized light signals were measured using a simplified and robust PEM-based polarimetric system which requires only a single incident polarization configuration. The resultant high-SNR ability to detect faint polarization signals amid the large depolarizing background from highly turbid suspensions is an encouraging development for the challenging bulk tissue polarimetry applications currently pursued in our laboratory. Future phantom studies will use model media that better approximate tissue properties, including broader and more biologically relevant scatterer size distributions (polydispersed suspensions), aspherical scatterers, absorptive media, and refractive index effects. To assist these investigations, improved Monte Carlo modelling methods should also be developed to simulate polarized photon propagation in tissue and tissue-like media.

Funding. Canadian Institutes of Health Research (CIHR, PJT-156110); Natural Sciences and Engineering Research Council of Canada (RGPIN-2018-04930); New Frontiers in Research Fund (NFRFE-2019-01049).

Acknowledgment. The foundational contributions of Dr. Daniel Cote in developing the pol-MC code are gratefully acknowledged.

Disclosures. The authors declare no conflicts of interest.

Data availability. Data underlying the results presented in this paper are not publicly available at this time but may be obtained from the authors upon reasonable request.

References

1. D. Bicout and C. Brosseau, "Multiply scattered waves through a spatially random medium: entropy production and depolarization," J. Phys. I **2**(11), 2047–2063 (1992).
2. N. Ghosh and I. A. Vitkin, "Tissue polarimetry: concepts, challenges, applications, and outlook," J. Biomed. Opt. **16**(11), 110801 (2011).
3. S. Alali and A. Vitkin, "Polarized light imaging in biomedicine: emerging Mueller matrix methodologies for bulk tissue assessment," J. Biomed. Opt. **20**(6), 061104 (2015).
4. R. H. Riddell, H. Goldman, D. F. Ransohoff, H. D. Appelman, C. M. Fenoglio, R. C. Haggitt, C. Hren, P. Correa, S. R. Hamilton, B. C. Morson, S. C. Sommers, and J. H. Yardley, "Dysplasia in inflammatory bowel disease: Standardized classification with provisional clinical applications," Hum. Pathol. **14**(11), 931–968 (1983).
5. V. Backman, R. Gurjar, K. Badizadegan, I. Itzkan, R. R. Dasari, L. T. Perelman, and M. S. Feld, "Polarized light scattering spectroscopy for quantitative measurement of epithelial cellular structures in situ," IEEE J. Sel. Top. Quantum Electron. **5**(4), 1019–1026 (1999).

Biomedical Optics EXPRESS

6. R. S. Gurjar, V. Backman, L. T. Perelman, I. Georgakoudi, K. Badizadegan, I. Itzkan, R. R. Dasari, and M. S. Feld, "Imaging human epithelial properties with polarized light-scattering spectroscopy," Nat. Med. **7**(11), 1245–1248 (2001).
7. T. Collier, M. Follen, A. Malpica, and R. Richards-Kortum, "Sources of scattering in cervical tissue: determination of the scattering coefficient by confocal microscopy," Appl. Opt. **44**(11), 2072 (2005).
8. A. Waldmann, S. Nolte, A. C. Geller, A. Katalinic, M. A. Weinstock, B. Volkmer, R. Greinert, and E. W. Breitbart, "Frequency of excisions and yields of malignant skin tumors in a population-based screening intervention of 360 288 whole-body examinations," Arch. Dermatol. **148**(8), 903–910 (2012).
9. J. G. Elmore, R. L. Barnhill, D. E. Elder, G. M. Longton, M. S. Pepe, L. M. Reisch, P. A. Carney, L. J. Titus, H. D. Nelson, T. Onega, A. N. A. Tosteson, M. A. Weinstock, S. R. Knezevich, and M. W. Piepkorn, "Pathologists' diagnosis of invasive melanoma and melanocytic proliferations: Observer accuracy and reproducibility study," BMJ **357**, j2813 (2017).
10. S. S. Lucky, K. C. Soo, and Y. Zhang, "Nanoparticles in photodynamic therapy," Chem. Rev. **115**(4), 1990–2042 (2015).
11. Y. Yang, Y. Hu, H. Du, and H. Wang, "Intracellular gold nanoparticle aggregation and their potential applications in photodynamic therapy," Chem. Commun. **50**(55), 7287–7290 (2014).
12. F. C. MacKintosh, J. X. Zhu, D. J. Pine, and D. A. Weitz, "Polarization memory of multiply scattered light," Phys. Rev. B **40**(13), 9342–9345 (1989).
13. K. M. Yoo and R. R. Alfano, "Time resolved depolarization of multiple backscattered light from random media," Phys. Lett. A **142**(8-9), 531–536 (1989).
14. J. M. Schmitt, A. H. Gandjbakhche, and R. F. Bonner, "Use of polarized light to discriminate short-path photons in a multiply scattering medium," Appl. Opt. **31**(30), 6535 (1992).
15. X. Ni and R. R. Alfano, "Time-resolved backscattering of circularly and linearly polarized light in a turbid medium," Opt. Lett. **29**(23), 2773 (2004).
16. E. E. Gorodnichev, A. I. Kuzovlev, and D. B. Rogozkin, "Diffusion of circularly polarized light in a disordered medium with large-scale inhomogeneities," JETP Lett. **68**(1), 22–28 (1998).
17. M. Xu and R. R. Alfano, "Circular polarization memory of light," Phys. Rev. E **72**(6), 065601 (2005).
18. M. Xu and R. R. Alfano, "Random walk of polarized light in turbid media," Phys. Rev. Lett. **95**(21), 213901 (2005).
19. M. J. Raković, G. W. Kattawar, M. Mehrűbeoğlu, B. D. Cameron, L. V. Wang, S. Rastegar, and G. L. Coté, "Light backscattering polarization patterns from turbid media: theory and experiment," Appl. Opt. **38**(15), 3399 (1999).
20. E. E. Gorodnichev, A. I. Kuzovlev, and D. B. Rogozkin, "Coherent backscattering of polarized light from a turbid medium," J. Exp. Theor. Phys. **106**(4), 731–743 (2008).
21. E. E. Gorodnichev, A. I. Kuzovlev, and D. B. Rogozkin, "Depolarization coefficients of light in multiply scattering media," Phys. Rev. E **90**(4), 043205 (2014).
22. R. C. N. Studinski and I. A. Vitkin, "Methodology for examining polarized light interactions with tissues and tissuelike media in the exact backscattering direction," J. Biomed. Opt. **5**(3), 330 (2000).
23. A. D. Kim and M. Moscoso, "Backscattering of circularly polarized pulses," Opt. Lett. **27**(18), 1589 (2002).
24. Y. L. Kim, P. Pradhan, M. H. Kim, and V. Backman, "Circular polarization memory effect in low-coherence enhanced backscattering of light," Opt. Lett. **31**(18), 2744 (2006).
25. D. Bicout, C. Brosseau, A. S. Martinez, and J. M. Schmitt, "Depolarization of multiply scattered waves by spherical diffusers: Influence of the size parameter," Phys. Rev. E **49**(2), 1767–1770 (1994).
26. V. Kuzmin and I. Meglinski, "Helicity flip of the backscattered circular polarized light," in *Biomedical Applications of Light Scattering IV*, A. P. Wax and V. Backman, eds. (2010), 7573(February 2010), p. 75730Z.
27. N. Ghosh, P. K. Gupta, H. S. Patel, B. Jain, and B. N. Singh, "Depolarization of light in tissue phantoms–effect of collection geometry," Opt. Commun. **222**(1-6), 93–100 (2003).
28. A. D. Kim and M. Moscoso, "Influence of the relative refractive index on the depolarization of multiply scattered waves," Phys. Rev. E: Stat. Phys., Plasmas, Fluids, Relat. Interdiscip. Top. **64**(2), 5 (2001).
29. M. Ahmad, S. Alali, A. Kim, M. F. G. Wood, M. Ikram, and I. A. Vitkin, "Do different turbid media with matched bulk optical properties also exhibit similar polarization properties?" Biomed. Opt. Express **2**(12), 3248 (2011).
30. Y. Piederrière, F. Boulvert, J. Cariou, B. Le Jeune, Y. Guern, and G. Le Brun, "Backscattered speckle size as a function of polarization: influence of particle-size and- concentration," Opt. Express **13**(13), 5030 (2005).
31. F. Boulvert, Y. Piederrière, G. Le Brun, B. Le Jeune, and J. Cariou, "Comparison of entropy and polarization memory rate behaviors through a study of weakly-anisotropic depolarizing biotissues," Opt. Commun. **272**(2), 534–538 (2007).
32. T. Novikova, A. Pierangelo, S. Manhas, A. Benali, P. Validire, B. Gayet, and A. De Martino, "The origins of polarimetric image contrast between healthy and cancerous human colon tissue," Appl. Phys. Lett. **102**(24), 241103 (2013).
33. D. C. Louie, J. Phillips, L. Tchvialeva, S. Kalia, H. Lui, W. Wang, and T. K. Lee, "Degree of optical polarization as a tool for detecting melanoma: proof of principle," J. Biomed. Opt. **23**(12), 1 (2018).
34. D. C. Louie, L. Tchvialeva, S. Kalia, H. Lui, and T. K. Lee, "Constructing a portable optical polarimetry probe for in-vivo skin cancer detection," J. Biomed. Opt. **26**(03), 1–15 (2021).
35. V. Sankaran, K. Schönenberger, J. T. Walsh, and D. J. Maitland, "Polarization discrimination of coherently propagating light in turbid media," Appl. Opt. **38**(19), 4252 (1999).

Biomedical Optics EXPRESS

36. V. Sankaran, M. J. Everett, D. J. Maitland, and J. T. Walsh, "Comparison of polarized-light propagation in biological tissue and phantoms," Opt. Lett. **24**(15), 1044 (1999).
37. V. Sankaran, J. T. Walsh, and D. J. Maitland, "Comparative study of polarized light propagation in biologic tissues," J. Biomed. Opt. **7**(3), 300 (2002).
38. M. Xu and R. R. Alfano, "Light depolarization by tissue and phantoms," in *Optical Interactions with Tissue and Cells XVII*, S. L. Jacques and W. P. Roach, eds. (2006), 6084(March 2006), p. 60840T.
39. B. Kunnen, C. Macdonald, A. Doronin, S. Jacques, M. Eccles, and I. Meglinski, "Application of circularly polarized light for non-invasive diagnosis of cancerous tissues and turbid tissue-like scattering media," J. Biophotonics **8**(4), 317–323 (2015).
40. A. da Silva, P. Stahl, S. Rehn, I. Vanzetta, and C. Deumié, "Depth selectivity in biological tissues by polarization analysis of backscattered light," Opt. Complex Syst. **8172**, 817205 (2011).
41. A. da Silva, A. Planat-Chrétien, M. Berger, S. Rehn, J.-M. Dinten, and C. Deumié, "Probing biological tissues in depth with elliptically polarized light," in *Optics InfoBase Conference Papers*, P. Taroni and H. Dehghani, eds. (2013), p. 879904.
42. S. Sridhar and A. Da Silva, "Enhanced contrast and depth resolution in polarization imaging using elliptically polarized light," J. Biomed. Opt. **21**(7), 071107 (2016).
43. G. Mie, "Beiträge zur Optik trüber Medien, speziell kolloidaler Metallösungen," Ann. Phys. **330**(3), 377–445 (1908).
44. D. H. Goldstein, "Chapter 5: Stokes Polarization Parameters," in *Polarized Light* (CRC Press, 2017).
45. J. Badoz, "Mesures photoélectriques de faibles biréfringences et de très petits pouvoirs rotatoires," J. Phys. Appliquée **17**(S11), 143–149 (1956).
46. J. C. Kemp, "Piezo-optical birefringence modulators: new use for a long-known effect," J. Opt. Soc. Am. **59**(8), 950 (1969).
47. F. A. Modine and R. W. Major, "High frequency polarization modulation method for measuring optical rotation," Appl. Opt. **14**(3), 761 (1975).
48. J. C. Kemp, "Polarized light and its interaction with modulating devices," Hinds Instruments, Inc., Hillsboro, OR 27 (1987).
49. J. Badoz, M. Billardon, J. C. Canit, and M. F. Russel, "Sensitive devices to determine the state and degree of polarization of a light beam using a birefringence modulator," J. Opt. **8**(6), 373–384 (1977).
50. Standford Research Systems, "Model SR830 DSP Lock-In Amplifier," (2011).
51. A. J. Hunt and D. R. Huffman, "A new polarization-modulated light scattering instrument," Rev. Sci. Instrum. **44**(12), 1753–1762 (1973).
52. J. M. Bueno and P. Artal, "Double-pass imaging polarimetry in the human eye," Opt. Lett. **24**(1), 64 (1999).
53. H. Horinaka, M. Osawa, K. Hashimoto, K. Wada, and Y. Cho, "Extraction of quasi-straightforward-propagating photons from diffused light transmitting through a scattering medium by polarization modulation," Opt. Lett. **20**(13), 1501 (1995).
54. S. G. Demos and R. R. Alfano, "Temporal gating in highly scattering media by the degree of optical polarization," Opt. Lett. **21**(2), 161 (1996).
55. X. Wang, L. V. Wang, C.-W. Sun, and C.-C. Yang, "Polarized light propagation through scattering media: time-resolved Monte Carlo simulations and experiments," J. Biomed. Opt. **8**(4), 608 (2003).
56. J. C. Kemp and M. S. Barbour, "A photoelastic-modulator polarimeter at Pine Mountain Observatory," Publ. Astron. Soc. Pac. **93**, 521 (1981).
57. D. Côté and I. A. Vitkin, "Pol-MC: a three dimensional polarization sensitive Monte Carlo implementation for light propagation in tissue," http://www.novajo.ca/ont-canc-inst-biophotonics.
58. D. Cote and I. A. Vitkin, "Robust concentration determination of optically active molecules in turbid media with validated three-dimensional polarization sensitive Monte Carlo calculations," Opt. Express **13**(1), 148 (2005).
59. A. D. Kim and M. Moscoso, "Diffusion of Polarized Light," Multiscale Model. Simul. **9**(4), 1624–1645 (2011).
60. J. P. Dark and A. D. Kim, "Asymptotic theory of circular polarization memory," J. Opt. Soc. Am. A **34**(9), 1642 (2017).
61. X. Guo, M. F. G. Wood, and A. Vitkin, "A Monte Carlo study of penetration depth and sampling volume of polarized light in turbid media," Opt. Commun. **281**(3), 380–387 (2008).
62. S. L. Jacques, "Optical properties of biological tissues: a review," Phys. Med. Biol. **58**(11), R37–R61 (2013).